Orbital ordering of Ir-t_{2g} states in the double perovskite Sr_2CeIrO_6

Sudipta Kanungo[1], Kailash Mogare[1], Binghai Yan[1,2], Claudia Felser[1], and Martin Jansen[1,3,*]
[1] *Max-Planck-Institut fur Chemische Physik fester Stoffe, 01187 Dresden, Germany*
[2] *Max-Planck-Institut fur Physik komplexer Systeme, 01187, Dresden, Germany*
[3] *Max-Planck-Institut fur Festkorperforschung, 70569 Stuttgart, Germany*

(Dated: August 3, 2015)

The electronic and magnetic properties of monoclinic double perovskite Sr_2CeIrO_6 were examined based on both experiments and first-principles density functional theory calculations. From the calculations we conclude that low-spin-state Ir^{4+} ($5d^5$, S=$\frac{1}{2}$) shows t_{2g} band derived anti-ferro type orbital ordering implying alternating occupations of d_{yz} and d_{xz} orbitals at the two symmetrically independent Ir sites. The experimentally determined Jahn-Teller type distorted monoclinic structure is consistent with the proposed orbital ordering picture. Surprisingly, the Ir-$5d$ orbital magnetic moment was found to be ≈ 1.3 times larger than the spin magnetic moment. The experimentally observed AFM-insulating states are consistent with the calculations. Both electron-electron correlation and spin-orbit coupling (SOC) are required to drive the experimentally observed AFM-insulating ground state. This single active site double perovskite provides a rare platform with a prototype geometrically frustrated fcc lattice where among the different degrees of freedom (i.e spin, orbital, and lattice), spin-orbit interaction and Coulomb correlation energy scales compete and interact with each other.

PACS numbers: 71.15.Mb, 71.20.Be, 75.25.Dk, 71.70.Ej

Transition metal oxides (TMOs) with orbitally degenerate d electrons exhibit rich electronic and magnetic properties arising from the interplay of spin, orbital, charge, and lattice degrees of freedom. When the number of d electrons (or holes) in a transition metal is smaller than the degeneracy of d orbitals, the d electrons have the freedom to occupy any of them. In such cases, the occupation of d orbitals at one site is often correlated with the occupation at the next site. Therefore, analogous to spin ordering, the orbital degrees of freedom can be locked and particular orbitals are occupied at each site, which is called orbital ordering. This orbital ordering, generally results from the interplay between structural distortion and Coulomb correlation of electrons. Orbital degrees of freedom often couple with spin degrees of freedom[1] and give rise to anisotropic electronic and magnetic interactions. Due to strong correlations between different degrees of freedom, orbital ordering spontaneously drive various exotic phenomena such as reduced dimensionality[1], structural phase transition[2], exotic magnetism[3], Peierls transitions[4], charge ordering[5] and orbital ordering induced ferroelectricity[6].

The possibility of orbital ordering has been discussed for doubly degenerate e_g orbitals of perovskite manganites[7], cuprates[1, 8] and for the degenerate t_{2g} orbitals of vanadates[9, 10]. Most studies investigating this aspect have focused on $3d$ TMOs; much less is known about whether related $4d$ and $5d$ oxides can exhibits similar behaviour. Recently, $4d$ and $5d$ TMOs have generated significant excitement because of the observation of unexpected orbital ordering[11] and localized transport properties and magnetism[12, 13] in ruthenate and iridate compounds, respectively. Due to the large spatial extension of $5d$ orbitals, the effects of electron correlation are weaker in $5d$ oxides than in $3d$ oxides, while the trend is opposite for the effects of spin-orbit coupling (SOC). Therefore, $5d$ oxides should exhibit a different balance among the effect of spin, orbital, and charge degrees of freedom. Although the importance of SOC in magnetic materials has been well known, the interplay between SOC and electronic Coulomb interactions in magnetic materials remains a largely unexplored field. The reason for this seems to be the mutually exclusive domain involved in their acting. It is only recently that this separation has been questioned[12–15].

The $5d$ double perovskite family is one of the most widely investigated oxides for studies exploring exotic phenomena such as magneto-optic effect[16], high-T_c ferrimagnets[17], half metallicity[18], peculiar AFM spin structures[19–21], as well as strong SOC driven phenomena such as spin liquid[22, 23], topological Mott insulator[15, 24] and the Weyl semimetal[25]. In the context of orbital ordering, $5d$ based systems have been less investigated, because generally for $5d$ elements such as Os, Ir, the SOC energy scale considerably exceeds the structural distortion energy scale. Strong SOC destroys orbitally degenerate electronic states required for orbital ordering. In this letter we report a particularly striking example of the interplay among SOC, Coulomb interactions and crystal field splitting in the double-perovskite Sr_2CeIrO_6, which shows a rare type of orbital ordering originating from the Ir-t_{2g} states. Using transport and magnetization measurements in addition to density-functional theory based first-principles calculations we explored this interesting aspect in the Sr_2CeIrO_6 double perovskite compound. We propose a rare case of t_{2g} orbitals derived anti-ferro type orbital ordering in this

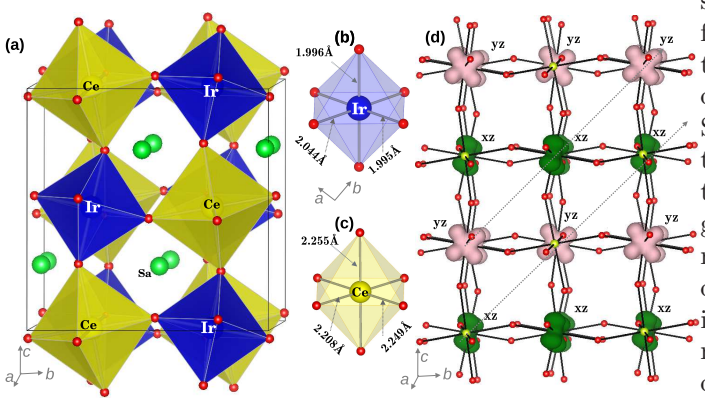

FIG. 1: (Color online)(a) Crystal structure of Sr_2CeIrO_6. Green, yellow, blue and red spheres represent Sr, Ce, Ir, and O atoms respectively. (b) and (c) Bond lengths marked octahedral entities of IrO_6 and CeO_6 respectively. (d) Three-dimensional magnetization density plot showing the orbital ordering. The orbital characters d_{yz} (pink surface) and d_{xz} (green surface) at each Ir site are marked. The isovalue was chosen to be 70 $e^-/\AA^3$. The dashed lines designate the orbital chains in the structure.

material at the Ir site with the half filled ($5d^5$) configuration while the Ce remains in the inert [Xe] configuration. Our proposed t_{2g} band derived anti-ferro orbital ordering constitute a strong contrast to the most widely known anti-ferro orbital ordering in $KCuF_3$[1] originated from the two e_g orbitals. Moreover only a few frustrated magnetic materials have been investigated in the context of orbital ordering, such as $NaNiO_2$[26], $LiNiO_2$[27, 28] and spinel ZnV_2O_4[29]. In this context Sr_2CeIrO_6 double perovskite is a rare example of a prototype geometrically frustrated fcc lattice where orbital ordering plays a crucial role. Our calculations revealed that the experimentally observed AFM insulating ground state is driven by strong SOC in addition to small onsite electron-electron Coulomb correlation at the Ir site. These particular behaviours make this system a potential candidate for investigating the interplay among the multiple degrees of freedom, such as spin, orbital, lattice, and multiple energy scales e.g. SOC and Coulomb correlations, that interact and compete with each others.

Sr_2CeIrO_6 crystallized in a monoclinic crystal structure with space group $P2_1/n$, with the lattice parameters a =5.8255 $\AA$, b = 5.8445 $\AA$, c = 8.2435 $\AA$ and β= 90.17^o, these values are very similar to the reported structure[30]. Due to lack of sensitiveness of positions of light atoms such as oxygen in X-ray diffractions based structural analysis, the theoretically optimized structure of Sr_2CeIrO_6 was obtained by relaxing the atomic positions of all atoms while keeping the lattice parameters fixed at the experimentally determined values. The structure consists of alternating corner sharing IrO_6 and CeO_6 octahedra, in all directions, as shown in Fig. 1(a). The Sr atoms are situated at the void positions between the two types of octahedra. Both IrO_6 and CeO_6 are distorted, the respective six metal-oxygens bond lengths are grouped into three values as shown in Figs. 1 (b) and (c) respectively. Interestingly the in-plane Ir-O bond lengths of two neighbouring IrO_6 octahedra are of opposite type, i.e the short in-plane Ir-O bond of one octahedron corresponds to the long in-plane bond of the neighbouring octahedron. Though the positions of the oxygen atoms shifts in the optimized structure compared to the experimental values, the average Ir-O and Ce-O bond lengths of the theoretically optimized structure (2.011 $\AA$ and 2.237 $\AA$ respectively) are in good agreement with the experimental average Ir-O (2.009 $\AA$) and Ce-O (2.202 $\AA$) bond lengths.

The magnetic susceptibilities of Sr_2CeIrO_6 were measured using a SQUID magnetometer (Quantum Design, MPMS MultiVu Application) in the temperature range from 2 to 300 K in varying field's up to 7 T, see Fig. 2. Inverse magnetic susceptibility data indicated AFM ordering at about 21 K. Fitting the high-temperature susceptibility to the Curie-Weiss law [$\chi = \frac{c}{T-\theta}$], gave μ^{eff}= 1.59 μ_B with a Weiss constant of θ= -108 K, which are very similar to the previously recorded values[30]. A negative value of θ implies dominant AFM interactions in the system. The observed effective magnetic moment indicates, that $Ir^{4+}(d^5)$ is in S=$\frac{1}{2}$ low-spin state and that μ^{eff} is somewhat smaller than the expected spin-only contribution [$\sqrt{S(S+1)}$] for the S=$\frac{1}{2}$ state. The inset of Fig. 2 shows the exponential decay of the resistivity as a function of temperature measured in a 0.01 T field with the Quantum Design PPMS MultiVu Application. Fitting the high temperature resistivity data with the semiconducting hopping mechanism, $\rho = \rho_0 e^{\frac{E_g}{2K_BT}}$, resulted in a bulk band gap (E_g) of $\approx$ 0.3 eV, indicating small gap insulating behaviour of this material.

The calculated ferromagnetic (FM), GGA+U density of states (DOS) projected on to Ir-5d states is shown in the top left panel of Fig. 3. The empty Sr states lay far away from the Fermi level (E_f), which is consistent with the nominal Sr^{2+} valence state. At the E_f only Ir-5d states contribute whereas the Ce-4f states are empty and situated far above the E_f, although Ir-5d states show significant mixing with the Ce-4f and O-2p states. We found that in the absence of on-site Coulomb correlation U, the band structure shows a metallic character. The incorporation of small Coulomb correlation $U_{eff} \geq 2$ eV at the Ir site, drove the insulating band structure. To clarify the effect of Coulomb correlation U on the electronic structure we systematically varied U^{Ir}_{eff} from 0 to 5 eV, as shown in Fig. S2 (in the supplemental mate-

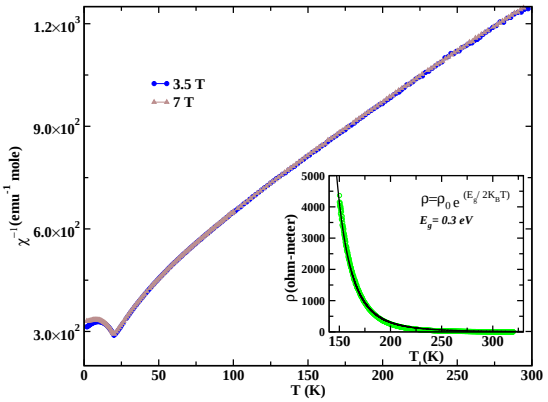

FIG. 2: (Color online)Temperature dependence of the inverse magnetic susceptibility of Sr_2CeIrO_6 measured at field strengths of 3.5 T and 7 T. The inset shows the temperature dependence of the resistivity measured in a 0.01 T field. The green (light) dots represent the experimental data while the solid line represents the fitting with exponential variation.

rial). The gap, and magnetic moments [0.63 μ_B (U^{Ir}_{eff} = 0 eV) to 0.86 μ_B (U^{Ir}_{eff} = 5 eV)] at Ir sites, increased with increasing U, while Ce stayed in the nonmagnetic state with zero magnetic moment. The orbital occupancies and spin states remained unchanged across the entire applied U range. Comparing our calculated band structure to the resistivity derived band gap, we choose to use U^{Ir}_{eff} = 3 eV (which, also is the commonly used U value for Ir in the literature[32]), for the following calculations. Because of the octahedral environment the five d states were broadly split into t_{2g} (d_{xy}, d_{yz}, d_{xz}) and e_g ($d_{3z^2-r^2}$, $d_{x^2-y^2}$) states as marked in the top left panel of Fig. 3. The Ir-t_{2g} states were completely filled in the majority spin channel and partially filled in the minority spin channel, whereas the Ir-e_g states were completely empty in both spin channels. These findings in addition to the calculated magnetic moment suggest that Ce is in the 4+ (Ce^{4+}:[Xe]) valence electronic state with zero magnetic moment in the inert configuration, and that Ir is in the 4+ ($5d^5$) low spin valence electronic state with S =$\frac{1}{2}$. These findings are consistent with the experimental magnetization measurements and previous electronic structure results[33]. However in the previous studies one failed to drive the insulating band structure without inclusion SOC.

Because of the octahedral distortion, the t_{2g} and e_g states are no longer degenerate. Contraction of IrO_6 octahedra along the c axis splits the triply degenerate t_{2g} states into a lower d_{xy} band (a_{1g} symmetry), and upper $d_{yz} - d_{xz}$ bands (e^{π}_g symmetry), as shown in the level diagram plot in the right top of Fig. 3. The d_{xy} band is filled in both spin channels and this is electronically inactive. The two e^{π}_g bands are filled by two majority spins and one minority spin, which results S=$\frac{1}{2}$ state. However the single minority spin has the freedom to occupy any orbital between the double degenerate $d_{yz} - d_{xz}$ bands. Therefore this minority spin experiences orbital degeneracy and drive a definite orbital ordering pattern in the lattice. To clarify this orbital degeneracy we plotted the orbital projected DOS for two Ir sites, Ir-1 (0.5, 0.0, 0.5) and Ir-2 (0.0, 0.5, 0.0), in the unit cell, as shown in the left middle and lower panels of Fig. 3 respectively. The plots show that the d_{yz} state of the Ir-1 site is equivalent to the d_{xz} state of the Ir-2 site, i.e. at the Ir-1 site the d_{xz} state is occupied while for the Ir-2 site, the d_{yz} state is populated by the single minority spin in the e^{π}_g bands, which is clearly shown in the energy level diagram of the respective right panels. To visualize the pattern of orbital ordering we plotted the magnetization density within GGA+U(U^{Ir}_{eff} = 3 eV) as shown in Fig.1(d). This figure shows that crystallographically two non-equivalent Ir sites, i.e Ir-1 and Ir-2 in the unit cell are decorated with the alternating d_{yz} and d_{xz} type orbitals and that these alternating orbital chains run along the body diagonal to the monoclinic unit cell. Because in this case the Ir sites prefer two different types of orbitals, we described this type of orbital ordering as anti-ferro type orbital ordering. Interesting point to be noted is that, aforementioned anti-ferro orbital ordering consisting of two t_{2g} orbitals is in contrast to the most widely known classic example of anti-ferro orbital ordering as found in $KCuF_3$[1], where alternating sites of Cu are occupied by the two e_g orbitals. Therefore Sr_2CeIrO_6 is a very unique case.

The resulted orbital ordering could be understood as an effect of the cooperative Jahn-Teller distortion associated to the IrO_6 octahedra. The individual IrO_6 octahedra are distorted as reflected by the three different types of Ir-O bond lengths in each octaherdon. If we concentrate only on the ab plane Ir-O bond lengths, theses are grouped into two Ir-O bond lengths as short 1.986 $\AA$ and long 2.033 $\AA$. However the crystallographic orientation of short and long bond lengths for the two Ir sites (i.e Ir-1 and Ir-2) are opposite. For Ir-1 the short bond (1.986 $\AA$) is along the crystallographic b axis and the long bond (2.033 $\AA$) along the crystallographic a axis, while for Ir-2, short bond is along the crystallographic a axis and long bond along the crystallographic b axis, i.e short bond of the Ir-1 octahedron corresponds to the long bond of the Ir-2 octahedron, see right middle and bottom panel of Fig. 3. Therefore this cooperative Jahn-Teller distortion in the IrO_6 octahedra, in terms of crystallographic orientation of Ir-O bond lengths, induces the occupation of two different orbitals in the two neighbouring distorted Ir octahedra.

To understand the role of SOC in this orbitally active material, we performed GGA+U+SOC (U^{Ir}_{eff} = 1-5 eV) calculations. Surprisingly we found that GGA+SOC without onsite U, could not drive the insulating nature of the band structure. We indeed required a small onsite correlation ($U^{Ir}_{eff} \geq 1$ eV) along with SOC to open

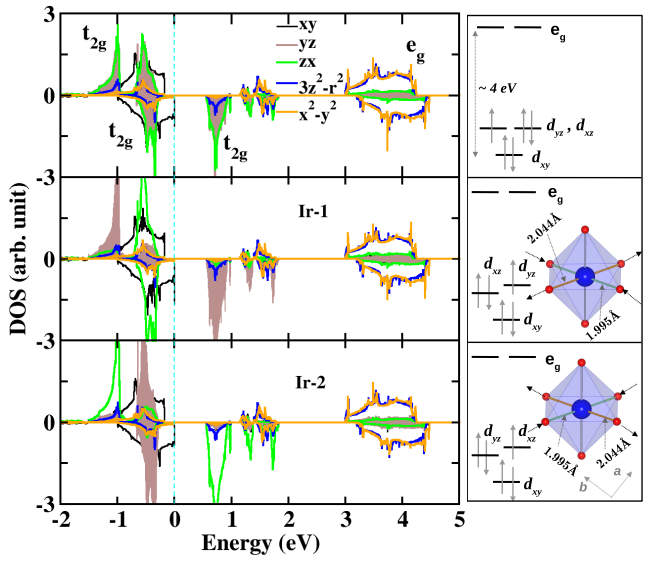

FIG. 3: (Color online) GGA+U(U^{Ir}_{eff} = 3 eV) FM spin-polarized Ir-5d orbital projected DOS. The two channels of the all panels represent majority and minority spin channels. The top panel represents the total Ir-d DOS in the unit cell while middle and lower panels represent the orbital projected DOS separately for the two Ir sites in the unit cell. The Fermi level is marked at zero on the energy scale. The right panels represent the energy level diagram corresponding to the left panel DOS. The individual IrO_6 octahera in the right panels are shown to clarify the bond length orientation in the crystallographic axes. In plane short (1.986 $\AA$) and long (2.033 $\AA$) bonds were marked by green and orange respectively. The arrow indicates the contraction and elongation of bond length along crystallographic axes.

an insulating gap in the band structure. Because of the orbital degeneracy of Ir, we found that orbital magnetic moment to be larger than the spin magnetic moment at the Ir site, although the value of the orbital and spin magnetic moments depended sensitively on chosen U values. For example, as we increased from a small value of U^{Ir}_{eff} = 1 eV [$\mu^{spin}(\mu^{orbital})$=0.25 (0.32) μ_B/Ir] to moderate value of U^{Ir}_{eff} = 3 eV [$\mu^{spin}(\mu^{orbital})$ = 0.33 (0.43) μ_B/Ir] to a large value of U^{Ir}_{eff} = 5 eV [$\mu^{spin}(\mu^{orbital})$=0.38 (0.53) μ_B/Ir], the spin, orbital moment and the ratio of $\mu^{orbital}/\mu^{spin}$ [1.28 (for U^{Ir}_{eff}= 1 eV), 1.34 (for U^{Ir}_{eff}= 3 eV), 1.39 (for U^{Ir}_{eff} =5 eV)] increased. We note that the orbital magnetic moments point in the same direction as the spin magnetic moment which is expected for the more than half filled t_{2g} occupancies at the Ir sites. Similarly large orbital magnetic moment and a similar $\mu^{orbital}/\mu^{spin}$ ratio are reported in the literature in the context of an other Ir based perovskite $BaIrO_3$[34]. We found that, in the GGA+U (U^{Ir}_{eff}=0-5 eV) calculations, FM alignment of Ir spins was energetically lower than the different possible AFM configurations. However experiments indicate a clear AFM transition at 17 K. Following the observation of significant orbital moments at both Ir sites, we investigated the possible role of SOC in the magnetic ground states. For this purpose, we conducted GGA+U+SOC calculations for FM and different AFM spin configurations. We found that, with the inclusion of SOC, compared to the other possible FM and AFM configurations, the A-type AFM state became the energetically lowest [$\mid E_{A-AFM} - E_{FM} \mid$= 2.8 meV/f.u] magnetic state. Our findings perfectly agree with previous electronic structure studies [33] as they also mentioned SOC driven stabilisation of the AFM state. In this A-AFM configuration, Ir spins are aligned ferromagnetically in the ab plane, and were coupled antiferromagnetically in the out-of-plane direction. We note that the experimental band gap ($\approx$ 0.3 eV) agrees qualitatively with the GGA+U+SOC (U^{Ir}_{eff} = 3 eV) AFM band gap ($\approx$ 0.35 eV). In Fig. S3 (in the supplementary material), we show the GGA+U and GGA+U+SOC band dispersion for the FM and AFM configurations. Because of the increase of Fermi energy for the AFM state over the FM state with the inclusion of SOC, the experimentally observed AFM state becomes energetically lower than the FM state. We confirmed the stability of the AFM state over FM configurations by cross checking our findings across the range of U^{Ir}_{eff} values from 1 to 5 eV, and we verified the existence of the proposed orbital ordering in the presence of AFM coupling as well. An interesting point to note is that, to obtain the correct magnetic ground state, the inclusion of SOC was mandatory, which reflects the importance of SOC in this Ir compound. We note a similar mechanism was recently suggested for other iridates[33, 35]. Therefore this material may be classified as a Coulomb enhanced SOC driven AFM insulator.

It is common believed that strong SOC destroys orbital ordering, however, the present material shows a rare exception. To understand the possible role of competition between SOC and structural distortion in deriving orbital ordering, we compare our results with the isoelectronic Ba variant (Ba_2CeIrO_6) of the present compound. Since Ba^{2+} has a larger radius the for the tolerance factor for the later (t=0.991) is close to 1. Therefore Ba form in an ideal cubic crystal structure [36] and the electronic structure does not allow a_{1g}-e^{π}_g splitting required for orbital ordering. Because of the smaller radius of Sr^{2+}, the tolerance factor (t=0.935) of Sr_2CeIrO_6 significantly deviates from 1 and thus a distorted monoclinic crystal structure results that allows the orbital ordering. From the total energy calculations we found that for Ba_2CeIrO_6, without inclusion of SOC, the monoclinic structure is lower (by 138 meV/f.u) than the cubic and we found similar orbital ordering as Sr_2CeIrO_6. However, inclusion of SOC cubic structure became $\approx$ 17 meV/f.u lower than the monoclinic. In contrast for the Sr_2CeIrO_6 both without and with SOC, the monoclinic structure is energetically $\approx$ 747 meV/f.u lower than than the cubic one. These analyses gave indirect evidence that, since

SOC energy scale remains unchanged between two compounds, in Sr_2CeIrO_6 the structural distortion is strong enough to overcome the negative SOC effect and we do obtain the orbital ordering state, which appears not to be possible for Ba_2CeIrO_6.

In conclusion, we conducted both experiments and DFT based first-principles calculations to investigate the nature of the orbital ordering in the ordered double perovskite Sr_2CeIrO_6, with Ir as a single electronically active site in the geometrically frustrated fcc lattice. We found t_{2g} band derived anti-ferro type of orbital ordering at the Ir site consisting of d_{yz} and d_{xz} orbitals that were associated by to alternating Ir sites along the body diagonal to the unit cell. Further experiments, such as X-ray resonant spectroscopy, would be helpful to directly probe our proposed orbital ordering pattern. We found that small electron-electron onsite correlation U is also relevant in this $5d$-Ir system for obtaining the correct insulating electronic structure. SOC played a very crucial role in this orbitally active material, for stabilizing the experimentally observed AFM ground state in addition to the small correlation effect, and with a large contribution of orbital magnetic moment greater than the spin counterpart. This Ir based double perovskite material has a very striking feature in which both electron-electron interaction and SOC energy scales are important for understanding the electronic and magnetic behaviour. More detailed experiments and theoretical analysis are required to explore this critical energy balance in this interesting material.

We thank the helpful discussions with Prof. J. van der Brink. This work is financially supported by the ERC Advanced Grant (Grant No. 291472)

* m.jansen@fkf.mpg.de

[1] K. I. Kugel *et al.*, Zh. Eksp. Teor. Fiz. **64**, 1429 (1973).
[2] Y. Tokunaga *et al.*, Nature Mater. **5**, 937 (2006).
[3] J. van den Brink *et al.*, Phys. Rev. Lett. **83**, 5118 (1999).
[4] D. I. Khomskii *et al.*, Phys. Rev. Lett. **94**, 156402 (2005).
[5] K. I. Kugel *et al.*, Physics-Uspekhi. **25**, 231 (1982).
[6] M. Imada *et al.* Rev. Mod. Phys. **70**, 1039 (1998).
[7] Y. Murakami, *et al.* Phys. Rev. Lett. **81**, 582 (1998).
[8] Y. Ito, *et al.* J. Phys. Soc. of Jpn. **40**, 1333 (1976).
[9] Y. Ren *et al.*, Nature (London) **396**, 441 (1998).
[10] S.-H. Lee *et al.*, Phys. Rev. Lett. **93**, 156407 (2004).
[11] P. Khalifah *et al.*, Science **297**, 2237 (2002).
[12] B. J. Kim *et al.* Phys. Rev. Lett. **101**, 076402 (2008).
[13] B. J. Kim *et al.*, Science **323**, 1329 (2009).
[14] S. J. Moon *et al.*, Phys. Rev. Lett. **101**, 226402 (2008).
[15] D. Pesin *et al.*, Nature Physics **6**, 376 (2010).
[16] H. Das *et al.*, Appl. Phys. Lett. **92**, 201912 (2008).
[17] Y. Krockenberger *et al.*, Phys. Rev. B **75**, 020404 (2007).
[18] J. B. Philipp *et al.*, Phys. Rev. B **68**, 144431 (2003).
[19] A. K. Paul *et al.*, Phys. Rev. Lett. **111**, 167205 (2013).
[20] B. Yan *et al.* Phys. Rev. Lett. **112**, 147202 (2014).
[21] S. Kanungo *et al.*, Phys. Rev. B **89**, 214414 (2014).
[22] W. Witczak-Krempa *et al.*, Ann. Rev. Cond. Matt. Phys. **5**, 57 (2014).
[23] Y. Okamoto *et al.*, Phys. Rev. Lett. **99**, 137207 (2007).
[24] B.-J. Yang *et al.*, Phys. Rev. B **82**, 085111 (2010).
[25] X. Wan *et al.*, Phys. Rev. B **83**, 205101 (2011).
[26] E. Chappel *et al.*, Eur. Phys. J. B **17**, 609 (2000).
[27] A. Rougier *et al.*, Solid state Commun. **94**, 123 (1995).
[28] J.-H. Chung *et al.*, Phys. Rev. B **71**, 064410 (2005).
[29] T. Mitra *et al.*, Phys. Rev. Lett. **99**, 126401 (2007).
[30] D. Harada *et. al.*, J. Solid. State Chem. **145**, 356 (1999).
[31] D. Harada *et. al.*, J. Phys.: Condens. Matter **12**, 3229 (2000).
[32] I. V. Solovyev *et. al.*, Phys. Rev. B **50**, 16861 (1994).
[33] S. K. Panda *et. al.*, Mod. Phys. Lett. B **27**, 1350041 (2013).
[34] M. A. Laguna-Marco *et. al.*, Phys. Rev. Lett. **105**, 216407 (2010).
[35] X. Ou *et al.*, Scientific Reports **4**, 4609 (2014).
[36] E. M. Ramos *et al.*, J. Material Science Lett. **14**, 1577 (1995).